ARTICLE IN PRESS

Computer Physics Communications ▮ (▮▮▮▮) ▮▮▮–▮▮▮

Contents lists available at ScienceDirect

Computer Physics Communications

journal homepage: www.elsevier.com/locate/cpc

Calculations of distance distributions and probabilities of binding by ligands between parallel plane membranes comprising receptors

Ianik Plante [a,*], Luc Devroye [b], Francis A. Cucinotta [c]

[a] Division of Space Life Sciences, Universities Space Research Association, 3600 Bay Area Boulevard, Houston, TX 77058, USA

[b] School of Computer Science, McGill University, 3480 University Street, Montreal H3A 0E9, Canada

[c] Department of Health Physics and Medical Diagnostics, University of Nevada Las Vegas, Las Vegas, NV 89154, USA

ARTICLE INFO

Article history:
Received 6 December 2012
Received in revised form
6 September 2013
Accepted 17 September 2013
Available online xxxx

Keywords:
Green's functions
Diffusion equation
Brownian dynamics algorithm
Monte Carlo simulations
Cell signaling
Non-targeted effects of radiation

ABSTRACT

Cell communication through biochemical signaling pathways is a key determinant of tissue responses to radiation. Several molecules, such as the transforming growth factor β (TGFβ), are implicated in radiation-induced signaling between cells. Brownian Dynamics (BD) algorithms have recently been used to simulate the interaction of ligands with receptors and to elucidate signal transduction and autocrine loops in ligand–receptors systems. In this paper, we discuss the simulation of particle diffusion and binding kinetics in a space bounded by two parallel plane membranes, using an exact algorithm to sample the propagator (Green's function) of a particle located between 2 membranes. We also show that the simulation results are independent of the number of time steps used, in accordance with time discretization equations. These simulations could be used to simulate the motion and binding of ligand molecules in a cell culture, and possibly in neuronal synapses.

1. Introduction

Many experiments have shown that cells may respond both collectively and individually to radiation [1,2] and that non-irradiated cells may be affected through signaling by those directly damaged by radiation [3]. Regarding this, non-targeted effects (NTE) refer to effects observed in cells not traversed by radiation, including in the progeny of cells many generations after exposure. A great number of NTEs have been observed, such as micronuclei formation, mutations, reduction in clonogenic survival, and apoptosis (reviewed in [4]). The mechanisms of NTE are poorly understood but several molecules such as the transforming growth factor (TGF-β) [5], reactive oxygen species (ROS) [6], NO$^{\cdot}$ radical [7], and membrane-bound NADPH oxidases [8] have been shown to be implicated in radiation-induced cell signaling. In particular, TGF-β is of great interest in radiobiology. This molecule is secreted by cells in an inactive or latent form, denoted as LTGF-β [9]. Latent TGF-β can be activated by many factors, notably by the $^{\cdot}$OH radicals produced by ionizing radiation [10]. After activation, TGF-β binds to membrane receptors and initiates a cascade of signaling events mediated by the Smad proteins [11]. Activated TGF-β has several effects on cells and is known to mediate cellular response to DNA damage [12] and to suppress apoptosis in irradiated cell cultures [5].

To investigate the mechanisms of cell signaling, computational models have been developed and applied to simulate the interaction between the epidermal growth factor (EGF) and its receptor (EFGR) in cell cultures [13–16]. These simulations use stochastic Brownian Dynamics (BD) algorithms to characterize the spatial range of secreted ligands and to discriminate the roles of autocrine and paracrine actions of ligands in cell culture. In a recent paper [17], we have developed exact BD algorithms based on analytical Green's functions of the diffusion equation (DE) to simulate the Brownian motion of a particle near a plane membrane with bound receptors and initiation of signal transduction by the ligand–receptor complex. In this paper, we present algorithms to sample the Green's functions of the DE of the Brownian motion of a molecule located between two parallel planes with receptors, which may be representative of cell cultures and possibly neuronal synapses. The algorithms have several advantages over those used in similar calculations [13], they are: (1) able to reproduce the exact distribution of particles predicted by the Green's functions for this problem; (2) efficient regarding computational speed and cost, and (3) can be used for any value of time step or position of a particle. Importantly, the time step does not need to be smaller when the particle is near the absorbing membrane. As in our previous paper [17], the Green's functions are presented first. Then,

* Correspondence to: NASA Johnson Space Center, 2101 NASA Parkway, Mail Code SK, Houston TX 77058, USA. Tel.: +1 281 244 6426; fax: +1 281 483 3058.
E-mail addresses: ianik.plante-1@nasa.gov (I. Plante), lucdevroye@gmail.com (L. Devroye), Francis.Cucinotta@unlv.edu (F.A. Cucinotta).

0010-4655/$ – see front matter © 2013 Elsevier B.V. All rights reserved.
http://dx.doi.org/10.1016/j.cpc.2013.09.011

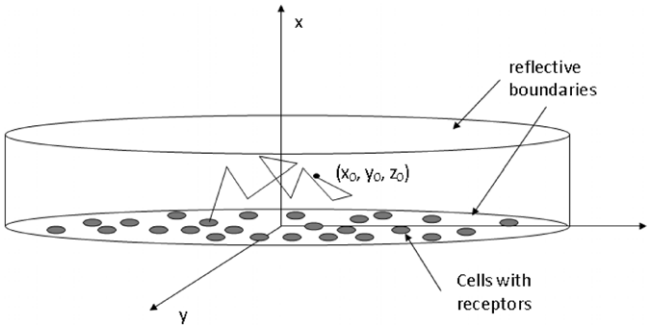

Fig. 1. 3D representation of ligand molecules in a cell culture. The cells are located at the bottom of the dish. A ligand initially at position (x_0, y_0, z_0) diffuses until it binds to a cell receptor.

we provide the time discretization equations and the sampling algorithms of the Green's functions. Finally, we present the results from our simulations and discuss how these simulations could be used to link radiation track structure models with existing DNA repair models to improve our understanding of the radiation risks.

2. Mathematical description

2.1. Description of the system

A ligand molecule is considered to be a particle located between two parallel membranes, that are described by the equations $x = 0$ and $x = L$ in Cartesian coordinates. The particle may diffuse freely in the directions Y and Z (i.e. no boundaries). This is illustrated in Fig. 1.

The trajectories of particles are obtained by randomly sampling the Green's function [18] of the diffusion equation (DE) in 3D:

$$\frac{\partial p(x, y, z, t \mid x_0, y_0, z_0)}{\partial t} = D\nabla^2 p(x, y, z, t \mid x_0, y_0, z_0), \tag{1}$$

where D is the diffusion coefficient, (x_0, y_0, z_0) is the initial position of the particle, (x, y, z) is a position in space, $p(x, y, z, t \mid x_0, y_0, z_0)$ is the Green's function of the DE (also called the *Brownian propagator*), t is the time and ∇^2 is the Laplacian. The initial condition is $p(x, y, z, t = 0 \mid x_0, y_0, z_0) = \delta(x - x_0)\delta(y - y_0)\delta(z - z_0)$, where $\delta(x)$ is the Dirac's delta function. In our system, $p(x, y, z, t \mid x_0, y_0, z_0)$ can be written as [19]:

$$p(x, y, z, t \mid x_0, y_0, z_0) = p_x(x, t \mid x_0)p_y(y, t \mid y_0)p_z(z, t \mid z_0), \tag{2}$$

where $p_x(x, t \mid x_0)$, $p_y(y, t \mid y_0)$ and $p_z(z, t \mid z_0)$ are solutions of their respective 1D diffusion equations:

$$\frac{\partial p_x(x, t \mid x_0)}{\partial t} = D\frac{\partial^2}{\partial x^2}p_x(x, t \mid x_0), \tag{3a}$$

$$\frac{\partial p_y(y, t \mid y_0)}{\partial t} = D\frac{\partial^2}{\partial y^2}p_y(y, t \mid y_0), \tag{3b}$$

$$\frac{\partial p_z(z, t \mid z_0)}{\partial t} = D\frac{\partial^2}{\partial z^2}p_z(z, t \mid z_0). \tag{3c}$$

Since the boundary conditions in the direction Y are $p_y(y \to \infty, t \mid y_0) \to 0$ and $p_y(y \to -\infty, t \mid y_0) \to 0$, and similar boundary conditions apply in the direction Z, $p_y(y, t \mid y_0)$ and $p_z(z, t \mid z_0)$ are Gaussian functions with variance $\sigma^2 = 2Dt$ and mean $\mu = y_0$ and $\mu = z_0$:

$$p_y(y, t \mid y_0) = \frac{1}{\sqrt{4\pi Dt}} \exp\left[-(y - y_0)^2/4Dt\right], \tag{4a}$$

$$p_z(z, t \mid z_0) = \frac{1}{\sqrt{4\pi Dt}} \exp\left[-(z - z_0)^2/4Dt\right]. \tag{4b}$$

As the diffusion in the directions Y and Z is independent from the diffusion in the direction X, only $p_x(x, t \mid x_0)$ is considered in the following discussion. In this paper, we considered two cases: (1) two reflecting membranes (at $x = 0$ and $x = L$) and (2) partially absorbing membrane at $x = 0$ and reflecting membrane at $x = L$.

2.2. Two reflecting plane membranes

The boundary conditions for a particle located between reflective membranes at $x = 0$ and $x = L$ are written as:

$$D\left.\frac{\partial p_x(x, t \mid x_0)}{\partial x}\right|_{x=0} = 0, \tag{5a}$$

$$D\left.\frac{\partial p_x(x, t \mid x_0)}{\partial x}\right|_{x=L} = 0. \tag{5b}$$

2.2.1. Green's function

The Green's function of the DE for the system with the boundary conditions given by Eq. (5) is [18,19]:

$$\begin{aligned} p_x(x, t \mid x_0) &= \frac{1}{L}\left(1 + 2\sum_{n=1}^{\infty} e^{-\pi^2 n^2 Dt/L^2} \cos\frac{n\pi x}{L} \cos\frac{n\pi x_0}{L}\right) \\ &\equiv \frac{1}{L}\sum_{n=-\infty}^{\infty} e^{-\pi^2 n^2 Dt/L^2} \cos\frac{n\pi x}{L} \cos\frac{n\pi x_0}{L}. \end{aligned} \tag{6}$$

This function is complicated by the presence of an infinite sum and may converge slowly for small values of t. It can be written in an equivalent form by using the Jacobi theta function

$$\theta(x) = \sum_{n=-\infty}^{\infty} \exp(-n^2\pi x), \quad x > 0. \tag{7}$$

This function has the remarkable property that $\sqrt{x}\theta(x) = \theta(1/x)$, which follows from the Poisson summation formula. In particular, Jacobi's theta function identity can be written:

$$\begin{aligned} &\frac{1}{\sqrt{\pi x}}\sum_{n=-\infty}^{\infty} \exp\left[-\frac{(n + y)^2}{x}\right] \\ &= \sum_{n=-\infty}^{\infty} \cos(2\pi nx) \exp(-n^2\pi x), \quad y \in \Re,\ x > 0. \end{aligned} \tag{8}$$

Using trigonometric identities, Eq. (6) can be written as:

$$\begin{aligned} p_x(x, t \mid x_0) = \frac{1}{L}\sum_{n=-\infty}^{\infty} &e^{-\pi^2 n^2 Dt/L^2} \\ &\times \left[\cos\frac{2\pi n(x + x_0)}{2L} + \cos\frac{2\pi n(x - x_0)}{2L}\right]. \end{aligned} \tag{9}$$

The application of Jacobi's theta function identity on Eq. (9) yields:

$$\begin{aligned} &p_x(x, t \mid x_0) \\ &= \frac{1}{\sqrt{4\pi Dt}}\sum_{n=-\infty}^{\infty}\left[e^{-(x - x_0 - 2nL)^2/4Dt} + e^{-(x + x_0 - 2nL)^2/4Dt}\right]. \end{aligned} \tag{10}$$

Therefore, $p_x(x, t \mid x_0)$ can also be expressed as an infinite sum of Gaussian functions.

Please cite this article in press as: I. Plante, et al., Calculations of distance distributions and probabilities of binding by ligands between parallel plane membranes comprising receptors, Computer Physics Communications (2013), http://dx.doi.org/10.1016/j.cpc.2013.09.011

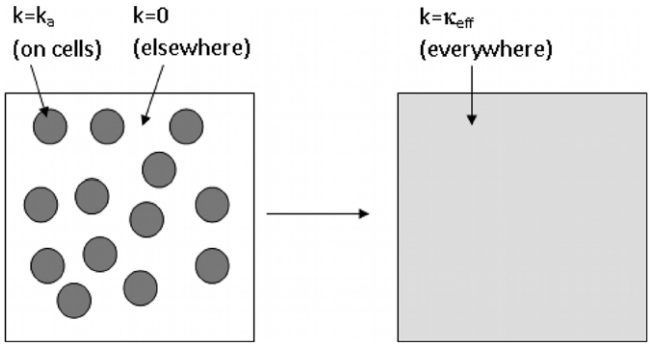

Fig. 2. Boundary homogenization procedure. As the receptors are present only on cell membranes, the surface rate constant $k = k_a$ on cell surfaces (approximated by disks) and $k = 0$ elsewhere. In our simulations, we assume that the receptors are distributed uniformly on the whole surface. Therefore, the rate constant of the surface can be estimated as κ_{eff}.

2.2.2. Survival probability

The survival probability of a free particle, denoted $Q(t \mid x_0)$, is calculated by integrating $p_x(x, t \mid x_0)$ over $[0, L]$:

$$\begin{aligned} Q(t \mid x_0) &= \int_0^L p_x(x, t \mid x_0)dx \\ &= \int_0^L \frac{1}{L}\left(1 + 2\sum_{n=1}^{\infty} e^{-\pi^2 n^2 Dt/L^2} \right. \\ &\quad \left. \times \cos\frac{n\pi x}{L}\cos\frac{n\pi x_0}{L}\right)dx = 1. \end{aligned} \tag{11}$$

The survival probability, as expected, is 1 in this case.

2.2.3. Asymptotic behavior

When $t \to \infty$, $p_x(x, t \to \infty \mid x_0) = 1/L$ which is the uniform probability distribution. This confirms that a uniform concentration of particles between the membranes is obtained when $Dt \gg L^2$.

2.2.4. Limit $L \to \infty$

When $L \to \infty$, $x \ll L$, $x_0 \ll L$ and $Dt \ll L^2$, the boundary at $x = L$ is too far to influence the Brownian motion of the particles. Indeed, all the terms in the summation of Eq. (10) are negligible (except $n = 0$), because of the dominant term $-n^2L^2$ in the exponential functions. Therefore, $p_x(x, t \mid x_0)$ reduces to

$$p_x(x, t \mid x_0) = \frac{1}{\sqrt{4\pi Dt}}\left[e^{-(x-x_0)^2/4Dt} + e^{-(x+x_0)^2/4Dt}\right]. \tag{12}$$

This is the Green's function for a particle near a reflective boundary at $x = 0$ (Ref. [17]).

2.3. Partially absorbing membrane at $x = 0$, reflecting membrane at $x = L$

After reviewing the Green's function of a particle between two reflecting plane membranes, we studied the case of a partially absorbing membrane at $x = 0$ and a reflecting membrane at $x = L$. This model system was used in Refs. [13,15] to simulate the accumulation of a ligand molecule in a cell culture.

The boundary conditions at $x = 0$ and $x = L$[1] are

$$D\left.\frac{\partial p_x(x, t \mid x_0)}{\partial x}\right|_{x=0} = k_1 p_x(0, t \mid x_0), \tag{13a}$$

$$D\left.\frac{\partial p_x(x, t \mid x_0)}{\partial x}\right|_{x=L} = 0. \tag{13b}$$

where $k_1 (> 0)$ is the absorption rate constant of the membrane at $x = 0$. In models representative of cell cultures, k_1 is an effective rate constant calculated with the ligand–receptor association rate constant, the number of receptors per cell and the fraction of the surface covered by cells, as shown in Fig. 2 [13–15,17].

2.3.1. Green's function

The Green's function of the DE with the boundary conditions (13a) and (13b) is [18]:

$$p_x(x, t \mid x_0) = \sum_{n=1}^{\infty} Z_n(x)Z_n(x_0)e^{-\alpha_n^2 Dt}, \tag{14}$$

where

$$Z_n(x) = \frac{\sqrt{2}\left[D\alpha_n\cos(\alpha_n x) + k_1\sin(\alpha_n x)\right]}{\sqrt{\left(D^2\alpha_n^2 + k_1^2\right)L + Dk_1}}, \tag{15}$$

and $\pm\alpha_n$, $n = 1, 2, \ldots$, are the roots of

$$\tan(\alpha L) = \frac{k_1}{D\alpha}. \tag{16}$$

The roots of Eq. (16) are shown in Fig. 3.

Using trigonometric identities and Eq. (16), it may be shown that

$$\cos(\alpha_n L) = \frac{D\alpha_n}{\sqrt{k_1^2 + D^2\alpha_n^2}}(-1)^{n+1}, \tag{17a}$$

$$\sin(\alpha_n L) = \frac{k_1}{\sqrt{k_1^2 + D^2\alpha_n^2}}(-1)^{n+1}. \tag{17b}$$

The factor $(-1)^{n+1}$ is introduced to account for the fact that the signs of $\cos(\alpha_n L)$ and $\sin(\alpha_n L)$ alternate (Fig. 3). For $k_1 = 0$, $\alpha_n = n\pi/L$; therefore, $Z_n(x) = \sqrt{2/L}\cos(n\pi x/L)$, and $p_x(x, t \mid x_0)$ takes the form given by Eq. (6).

2.3.2. Survival probability

The survival probability of a particle is obtained by integrating $p_x(x, t \mid x_0)$ over $[0, L]$:

$$\begin{aligned} Q(t \mid x_0) &= \int_0^L p_x(x, t \mid x_0)dx \\ &= \int_0^L \sum_{n=1}^{\infty} Z_n(x)Z_n(x_0)e^{-\alpha_n^2 Dt}dx \\ &= \sum_{n=1}^{\infty} Z_n(x_0)e^{-\alpha_n^2 Dt}\int_0^L Z_n(x)dx, \end{aligned} \tag{18}$$

$$\begin{aligned} Q(t \mid x_0) &= 2\sum_{n=1}^{\infty} \frac{\left[D\alpha_n\cos(\alpha_n x_0) + k_1\sin(\alpha_n x_0)\right]}{\sqrt{\left(D^2\alpha_n^2 + k_1^2\right)L + Dk_1}} \\ &\quad \times \frac{\left[D\sin(\alpha_n L) + k_1(1 - \cos(\alpha_n L))/\alpha_n\right]}{\sqrt{\left(D^2\alpha_n^2 + k_1^2\right)L + Dk_1}}e^{-\alpha_n^2 Dt}. \end{aligned} \tag{19}$$

This can also be written as:

$$\begin{aligned} Q(t \mid x_0) &= 2\sum_{n=1}^{\infty} \frac{\left[D\alpha_n\cos(\alpha_n x_0) + k_1\sin(\alpha_n x_0)\right]}{\left(D^2\alpha_n^2 + k_1^2\right)L + Dk_1}\frac{k_1}{\alpha_n}e^{-\alpha_n^2 Dt} \\ &= \sum_{n=1}^{\infty} Z_n(x_0)Z_n(0)\frac{k_1}{D^2\alpha_n^2}e^{-\alpha_n^2 Dt}. \end{aligned} \tag{20}$$

The probability of a particle to bind at the membrane $x = 0$, denoted $p(*, t \mid x_0)$, can be obtained either by integrating the flux of particles at $x = 0$ or by using the conservation equation $p(*, t \mid x_0) + Q(t \mid x_0) = 1$.

[1] It is also possible to introduce a rate constant (k_2) in the boundary condition at $x = L$. In this work, only the case with $k_2 = 0$ is considered.

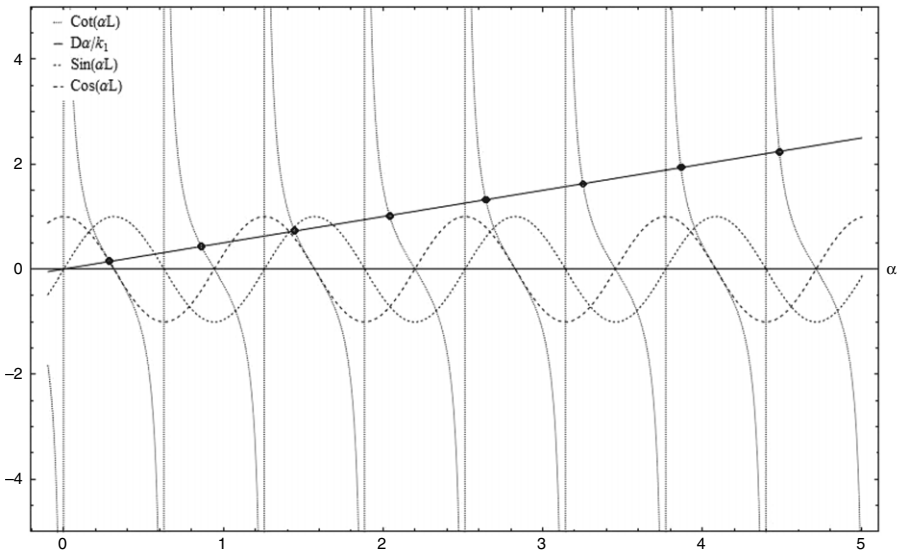

Fig. 3. Roots of Eq. (16) for $k_1 = 2$, $D = 1$ and $L = 5$. The roots are at the intersection of the curves and are marked by dots. The signs of $\sin(\alpha L)$ and $\cos(\alpha L)$ alternate.

3. Discretization of time

As discussed in our previous work on a particle near a plane membrane [17] and in simulation of chemical reactions [20,21], Brownian Dynamics simulations can be done in several time steps. Therefore, if $t = \Delta t_1 + \Delta t_2$, we should have:

$$p_x(x, t \mid x_0) = \int_\Omega p_x(x, \Delta t_2 \mid x_1) p_x(x_1, \Delta t_1 \mid x_0) dx_1, \tag{21}$$

where Ω is the domain of x_1, i.e. $[0, L]$ in the present case. This is the Chapman–Kolmogorov equation, which holds for Markov processes. That is, the probability for a particle initially at x_0 to end at position x is equivalent to the sum of all probabilities to go to an intermediate position x_1 and end at x.

3.1. Two reflecting membranes

Eq. (21) can be verified directly for two reflecting membranes:

$$I = \frac{1}{L^2} \int_0^L \left(\sum_{n=-\infty}^{\infty} e^{-\pi^2 n^2 D \Delta t_2 / L^2} \cos \frac{n\pi x}{L} \cos \frac{n\pi x_1}{L} \right) \times \left(\sum_{m=-\infty}^{\infty} e^{-\pi^2 m^2 D \Delta t_1 / L^2} \cos \frac{m\pi x_1}{L} \cos \frac{m\pi x_0}{L} \right) dx_1. \tag{22}$$

The integral can be rearranged by keeping the terms comprising the integration variable x_1:

$$I = \frac{1}{L} \sum_{n,m=-\infty}^{\infty} e^{-\pi^2 D (m^2 \Delta t_1 + n^2 \Delta t_2)/L^2} \cos \frac{n\pi x}{L} \cos \frac{m\pi x_0}{L} \times \frac{1}{L} \int_0^L \cos \frac{n\pi x_1}{L} \cos \frac{m\pi x_1}{L} dx_1. \tag{23}$$

The result of the integral is $\delta_{mn}/2$, but each term (except for $n = 0$) is counted twice in the double sum. For $n = 0$, the result is δ_{m0}, but it is counted once. Therefore the double sum can be reduced to a simple sum:

$$I = \frac{1}{L} \sum_{m-\infty}^{\infty} e^{-\pi^2 D m^2 (\Delta t_1 + \Delta t_2)/L^2} \cos \frac{m\pi x}{L} \cos \frac{m\pi x_0}{L} \equiv p_x(x, t \mid x_0). \tag{24}$$

This confirms the time discretization equation for the Green's function of a particle between two reflecting membranes.

3.2. Partially absorbing membrane at $x = 0$, reflecting membrane at $x = L$

A free particle initially located at x_0 at $t = 0$ can either (i) go to an intermediate position x_1 during Δt_1 and then go to its final x position at Δt_2, (ii) bind to the membrane during Δt_1, or (iii) go to an intermediate position x_1 during Δt_1 and bind to the membrane during Δt_2. The first possibility is described by Eq. (21). The probability to find a particle bound at $t = \Delta t_1 + \Delta t_2$ is given by the sum of (ii) and (iii):

$$p(*, t \mid x_0) = p(*, \Delta t_1 \mid x_0) + \int_\Omega p(*, \Delta t_2 \mid x_1) p_x(x_1, \Delta t_1 \mid x_0) dx_1, \tag{25}$$

where $p(*, t \mid x_0)$ is the probability of a particle initially at x_0 to bind to the membrane at $x = 0$ at time t. The time discretization equations can also be verified directly from the Green's functions in this case. For this system, Eq. (21) can be written:

$$I = \int_0^L \left(\sum_{n=1}^{\infty} Z_n(x) Z_n(x_1) e^{-\alpha_n^2 D \Delta t_2} \right) \times \left(\sum_{m=1}^{\infty} Z_m(x_1) Z_m(x_0) e^{-\alpha_m^2 D \Delta t_1} \right) dx_1, \tag{26}$$

$$I = \sum_{n,m=1}^{\infty} Z_n(x) Z_m(x_0) e^{-\alpha_n^2 D \Delta t_2} e^{-\alpha_m^2 D \Delta t_1} \times \int_0^L Z_n(x_1) Z_m(x_1) dx_1. \tag{27}$$

This integral is straightforward because it is composed of simple products of trigonometric functions. The result, given in the Appendix A, is δ_{mn}. Therefore

$$I = \sum_{n,m=1}^{\infty} Z_n(x) Z_m(x_0) e^{-\alpha_n^2 D \Delta t_2} e^{-\alpha_m^2 D \Delta t_1} \delta_{mn} = \sum_{m=1}^{\infty} Z_m(x) Z_m(x_0) e^{-\alpha_m^2 D (\Delta t_1 + \Delta t_2)} \equiv p_x(x, t \mid x_0). \tag{28}$$

As shown in our previous work [17,20], Eq. (25) can be deduced from Eq. (21). However, it is also possible to verify it directly from the Green's functions. Using the conservation equation

Please cite this article in press as: I. Plante, et al., Calculations of distance distributions and probabilities of binding by ligands between parallel plane membranes comprising receptors, Computer Physics Communications (2013), http://dx.doi.org/10.1016/j.cpc.2013.09.011

$p(*, t \mid x_0) + Q(t \mid x_0) = 1$, Eq. (25) can be written:

$$I = p(*, \Delta t_1 \mid x_0) + \int_0^L \left[1 - \sum_{n=1}^{\infty} Z_n(x_1) Z_n(0) \frac{k_1}{D^2 \alpha_n^2} e^{-\alpha_n^2 D \Delta t_2} \right] \times \left[\sum_{m=1}^{\infty} Z_m(x_1) Z_m(x_0) e^{-\alpha_m^2 D \Delta t_1} \right] dx_1. \quad (29)$$

The first term of the integral is $Q(\Delta t_1 \mid x_0)$:

$$I = p(*, \Delta t_1 \mid x_0) + Q(\Delta t_1 \mid x_0) - \sum_{n,m=1}^{\infty} e^{-\alpha_m^2 D \Delta t_1 - \alpha_n^2 D \Delta t_2} Z_m(x_0) Z_n(0) \frac{k_1}{D^2 \alpha_n^2} \times \int_0^L Z_m(x_1) Z_n(x_1) dx_1. \quad (30)$$

The result of the integral is δ_{mn} (Appendix A):

$$I = 1 - \sum_{n,m=1}^{\infty} e^{-\alpha_m^2 D \Delta t_1 - \alpha_n^2 D \Delta t_2} Z_m(x_0) Z_n(0) \frac{k_1}{D^2 \alpha_n^2} \delta_{mn} = 1 - \sum_{n=1}^{\infty} e^{-\alpha_n^2 D (\Delta t_1 + \Delta t_2)} Z_n(x_0) Z_n(0) \frac{k_1}{D^2 \alpha_n^2} \equiv p(*, \Delta t_1 + \Delta t_2 \mid x_0). \quad (31)$$

This confirms the time discretization equation for particle binding.

4. Sampling of the Green's functions (Brownian Dynamics algorithms)

In this section, we present Brownian Dynamics algorithms used to sample the position of a particle after one time step. The sampling of y and z distributed as $p_y(y, t \mid y_0)$ and $p_z(z, t \mid z_0)$ is done by using Gaussian random numbers of variance $\sigma^2 = 2D\Delta t$ and mean $\mu = y_0$ and $\mu = z_0$ (D is the diffusion coefficient of the particle and Δt is the time step). In the remainder of this section, we provide algorithms to generate x distributed as $p_x(x, t \mid x_0)$. These algorithms use the series method, which has been suggested by Devroye [22], and was further developed and analyzed in his book [23] and a paper [24]. The details are given in the supporting document (see Appendix B).

4.1. Two reflecting membranes

As seen in Section 2.2, the probability density $p_x(x, t \mid x_0)$ can have a flat or peaked shape, for which the sampling algorithms are to be different. The condition $L^2 \geq (Dt) \ln 2$ determines which algorithm is used.

4.1.1. Sampling algorithm for $p(x, t \mid x_0)$ for $L^2 \geq (Dt) \ln 2$

The algorithm presented in this section is only valid when the condition $L^2 \geq (Dt) \ln 2$ is satisfied. It is based on the fact that $p_x(x, t \mid x_0)$ can be expressed as a mixture of Gaussian functions (Section 2). The functions $a_n(x)$, $b_n(x)$ and $f^*(x)$ are defined as follow:

$$a_n(x) = \exp\left[-\frac{(2Ln + (x + x_0))^2}{4Dt} \right], \quad (32)$$

$$b_n(x) = \exp\left[-\frac{(2Ln + (x - x_0))^2}{4Dt} \right], \quad (33)$$

$$f^*(x) = \sum_{n=-\infty}^{\infty} (a_n(x) + b_n(x)). \quad (34)$$

Algorithm 1 is:

Algorithm 1A: Generation of random variate X distributed as $p_x(x, t \mid x_0)$ for $k_1 = k_2 = 0$ and $L^2 \geq (Dt) \ln 2$
REPEAT
{
GENERATE U, V uniform on [0, 1], N standard normal
IF (V < 2/9) THEN SET X ← 2L − x_0 + $\sqrt{2DtN}$
ELSE SET X ← x_0 + $\sqrt{2DtN}$
IF (0 ≤ X ≤ L) THEN SET Y ← U($7b_0$(X) + $2a_{-1}$(X))
}
UNTIL 0 ≤ X ≤ L and Y ≤ f^*(X)
RETURN X

The verification of the condition $Y \leq f^*(X)$ requires the evaluation of an infinite sum. However, it is possible to verify whether the condition is true without ever calculating the value of $f^*(X)$ exactly by using this algorithm:

Algorithm 1B: Verification of $Y < f^*(X)$
SET S ← a_0(X) + b_0(X), k ← 1 (S holds the approximation sum)
REPEAT FOREVER
{
T ← 2(a_k(X) + a_{-k}(X) + b_k(X) + b_{-k}(X))
IF (Y ≥ S + T) THEN RETURN "Y ≥ f^*(X)" and EXIT
IF (Y ≤ S − T) THEN RETURN "Y ≤ f^*(X)" and EXIT
S ← S + T/2
k ← k + 1
}

4.1.2. Sampling algorithm for $p_x(x, t \mid x_0)$ for $L^2 \leq (Dt) \ln 2$

In this section, we assume that the condition $L^2 \leq (Dt) \ln 2$ holds. However, the algorithm presented here is valid for all possible values of the parameters ($Dt > 0$, $L > 0$, and x and $x_0 \in [0, L]$). However, it is preferable to use *Algorithm* 1 if $L^2 > (Dt) \ln 2$, because it is more efficient if the condition is true. For this section, the functions $f(x)$ and $f_n(x)$ are defined:

$$f(x) = \frac{1}{L} + 2 \sum_{n=1}^{\infty} f_n(x), \quad (35)$$

and

$$f_n(x) \stackrel{\text{def}}{=} \frac{1}{L} e^{-\pi^2 n^2 Dt / L^2} \cos \frac{n\pi x}{L} \cos \frac{n\pi x_0}{L}. \quad (36)$$

The sampling algorithm is:

Algorithm 2A: Generation of random variate X distributed as $p_x(x, t \mid x_0)$ for $k_1 = k_2 = 0$
DEFINE H ← 1/L + $1/\sqrt{\pi Dt}$
REPEAT
{
GENERATE U, V uniform on [0, 1] and X uniform on [0, L]
SET Y ← VH
}
UNTIL Y ≤ f(X)
RETURN X

The verification of $Y \leq f(X)$ is dose by using the following routine:

Algorithm 2B: Verification of $Y < f(X)$
SET S ← 1/L + 2f$_1$(X), k ← 1 (S holds the approximation sum)
REPEAT FOREVER
{
T = L exp(−π²k²Dt/L²)/(π²kDt)
IF (Y ≥ S + T) THEN RETURN "Y ≥ f(X)" and EXIT
IF (Y ≤ S − T) THEN RETURN "Y ≤ f(X)" and EXIT
k ← k + 1
S ← S + 2f$_k$(X)
}

4.2. Partially absorbing membrane at $x = 0$, reflecting membrane at $x = L$

In this case, we need to generate random variates of the sub-density[2] given by Eq. (14). Random variate generation for this Green's function introduces a new problem; beyond the infinite sum there is the fact that none of the constants α_n can be computed exactly. Yet, it is possible to design an exact random variate generation without ever computing any α_n exactly. At first, $p_x(x, t \mid x_0)$ and $Q(t \mid x_0)$ can be written in this form by using trigonometric identities:

$$p_x(x, t \mid x_0) = \sum_{n=1}^{\infty} A_L(\alpha_n) \cos[\alpha_n(L - x)] \times \cos[\alpha_n(L - x_0)] e^{-\alpha_n^2 Dt}, \quad (37)$$

$$Q(t \mid x_0) = \sum_{n=1}^{\infty} A_L(\alpha_n) \sin(\alpha_n L) \cos[\alpha_n(L - x_0)] e^{-\alpha_n^2 Dt}/\alpha_n, \quad (38)$$

where

$$A_L(\alpha_n) = \frac{2\left(D^2\alpha_n^2 + k_1^2\right)}{\left(D^2\alpha_n^2 + k_1^2\right)L + Dk_1}. \quad (39)$$

The approximate values of the roots α_n used in the algorithm are given by $\alpha_{n,N}$, where the accuracy parameter N is an integer number larger than 1. Given N, $\alpha_{n,N}$ is obtained by a binary search such that

$$\alpha_n \le \alpha_{n,N} \le \min\left(\alpha_n + 2^{-N}, \frac{2n-1}{2}\pi\right). \quad (40)$$

The binary search tries to find the unique solution of $\tan(\alpha L) = k_1/D\alpha$ in the interval $[(2n-2)\pi/2L, (2n-1)\pi/2L]$ and clearly needs no more than N steps. The $\alpha_{n,N}$ are calculated for all $1 \le n \le N$, for a total computational cost of N^2. The N-th approximants of $p_x(x, t \mid x_0)$ and $Q(t \mid x_0)$, denoted $p_{x,N}(x, t \mid x_0)$ and $Q_N(t \mid x_0)$, are:

$$p_{x,N}(x, t \mid x_0) = \sum_{n=1}^{N} A_L(\alpha_{n,N}) \cos[\alpha_{n,N}(L - x)] \times \cos[\alpha_{n,N}(L - x_0)] e^{-\alpha_{n,N}^2 Dt}, \quad (41)$$

$$Q_N(t \mid x_0) = \sum_{n=1}^{N} A_L(\alpha_{n,N}) \sin(\alpha_{n,N} L) \times \cos[\alpha_{n,N}(L - x_0)] e^{-\alpha_{n,N}^2 Dt}/\alpha_{n,N}. \quad (42)$$

[2] A sub-density means that $P = \int_0^L f(x)dx \le 1$, and $f(x) \ge 0$. In this case, a random variate with the density f/P is generated with probability P.

In Appendix B, it is shown that $p_x(x, t \mid x_0) \le S^*$, where

$$S^* \stackrel{\text{def}}{=} \frac{2}{L}\left[e^{-Q^2 Dt} + \frac{L}{\sqrt{4\pi Dt}}\right], \quad (43)$$

and

$$Q \stackrel{\text{def}}{=} \frac{\pi k_1}{\pi D + 2Lk_1}. \quad (44)$$

For *Algorithm* 3, R_N and M are defined as:

$$R_N \stackrel{\text{def}}{=} \frac{L\exp(-Dt(N-1)^2\pi^2/L^2)}{(N-1)Dt\pi^2}, \quad (45)$$

$$M = 2\left(\frac{2L + 2L^2Q + \pi DtQ}{L^2Q}\right)\exp(-Q^2Dt) + 4\left(\frac{L/\pi + L + \pi Dt/2L}{\sqrt{4\pi Dt}} + \frac{L}{2\pi}\right). \quad (46)$$

The algorithm is:

Algorithm 3A: Generation of random variate X distributed as $p_x(x, t \mid x_0)$ for $k_1 > 0$, $k_2 = 0$
COMPUTE S*
REPEAT
{
GENERATE V uniform on [0, 1] and X uniform on [0, L]
SET Y ← VS*
}
UNTIL Y ≤ p(X)
RETURN X

The verification of $Y \le p(X)$ is done by using Algorithm 3B:

Algorithm 3B: Verification of $Y < p(X)$
SET N ← 2
REPEAT FOREVER
{
T ← R$_N$ + 2^{-N}M
IF (Y ≥ p$_{x,N}$(X) + T) THEN RETURN "Y > p(X)" and EXIT
IF (Y ≤ p$_{x,N}$(X) − T) THEN RETURN "Y ≤ p(X)" and EXIT
N ← N + 1
}

Finally, the survival of a particle is determined by sampling a Bernoulli random variate ξ with possible values 1 (survival) and 0 (binding). First define R_N^* and M^*:

$$R_N^* \stackrel{\text{def}}{=} \frac{L\exp(-Dt(N-1)^2\pi^2/L^2)}{N(N-1)Dt\pi^3}, \quad (47)$$

$$M^* = \left(\frac{3 + 2LQ + 2DtQ^2}{Q^2}\right)\frac{2}{L}\exp(-Q^2Dt) + \left(\frac{3L^2 + 2L^2\pi + 2Dt\pi^2}{\pi^2}\right)\frac{1}{\sqrt{\pi Dt}}. \quad (48)$$

The algorithm is:

Algorithm 4: Generation of a Bernoulli (P) random variate ξ
GENERATE U uniform on [0, 1]
SET N ← 2
REPEAT FOREVER:
{
T ← R$_N^*$ + 2^{-N}M*
IF (U > Q$_N$ + T) THEN RETURN $\xi = 0$
IF (U ≤ Q$_N$ − T) THEN RETURN $\xi = 1$
N ← N + 1
}

Please cite this article in press as: I. Plante, et al., Calculations of distance distributions and probabilities of binding by ligands between parallel plane membranes comprising receptors, Computer Physics Communications (2013), http://dx.doi.org/10.1016/j.cpc.2013.09.011

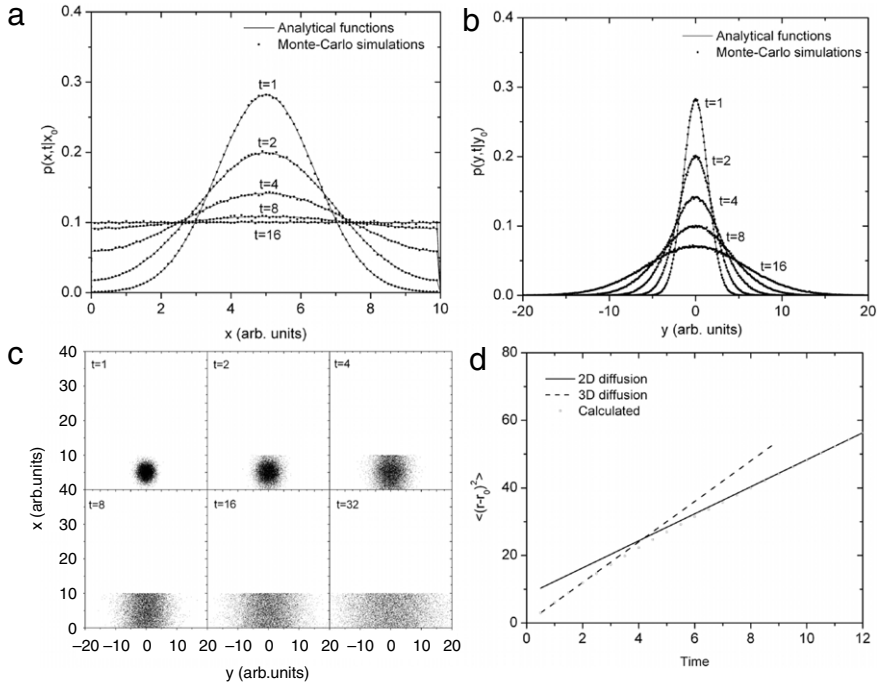

Fig. 4. Probability distributions $p_x(x, t \mid x_0)$ (panel a) and $p_y(y, t \mid y_0)$ (panel b) for particles initially at $(x_0 = 5, y_0 = 0, z_0 = 0)$, diffusing freely between two reflecting membranes at $x = 0$ and $x = L = 10$, at $t = 1, 2, 4, 8$ and 16 time units. (−): Analytical predictions; (■): Monte Carlo simulations using 1,000,000 particles. Panel c: projection in the XY plane of the positions of particles (only 3000 are shown) used for the simulations depicted in panels a and b at $t = 1, 2, 4, 8, 16$ and 32 units. Panel d: $\langle(\boldsymbol{r} - \boldsymbol{r}_0)^2\rangle$ as a function of time for the particles of Fig. 4(a) and (b).

5. Results and discussion

In this section, simulation results using the algorithms are presented.

5.1. Two reflecting membranes

In this case, the particles are located between reflecting membranes. To simplify the following discussion, only the distributions $p_x(x, t \mid x_0)$ and $p_y(y, t \mid y_0)$ will be shown, because $p_z(z, t \mid z_0)$ is similar to $p_y(y, t \mid y_0)$.

In Fig. 4(c), we show the diffusion of particles initially at $(x_0, y_0, z_0) = (5, 0, 0)$ between the plane membranes at $x = 0$ and $x = L = 10$, at $t = 1, 2, 4, 8, 16$ and 32 time units.[3] The positions of the particles after a time step Δt are obtained by using *Algorithm* 1 or *Algorithm* 2 in the direction X and by sampling Gaussian random numbers with variance $\sigma^2 = 2D\Delta t$ and mean $\mu = y_0$ and $\mu = z_0$ in the directions Y and Z. The coordinates of the particles are stored in histograms after the sampling and normalized to the initial number of particles, to obtain the distributions of the coordinates X, Y and Z. The distributions of the coordinates X and Y of the particles shown in Fig. 4(c) are plotted in Fig. 4(a) and (b) and compared with the analytical Green's functions.

With time, as expected, $p_x(x, t \mid x_0)$ becomes uniform. In the directions Y and Z, the distributions are Gaussians. The results are independent of the number of time steps used for the simulation (results not shown), in accordance with the time discretization equations.

To further validate *Algorithm* 1 and *Algorithm* 2, we performed a simulation with membranes at $x = 0$ and $x = L = 100$, for particles at $(x_0, y_0, z_0) = (1, 0, 0)$, and using $t = 1, 2, 4, 8$ and 16 units. In this case, $x \ll L, x_0 \ll L$ and $Dt \ll L^2$; therefore, $p_x(x, t \mid x_0)$ can be approximated by Eq. (12), which is the well known Green's function for particles near a reflective boundary [17]. No significant difference was observed when the distributions of the coordinates X of the particles were compared to those predicted by Eq. (12) (results not shown).

5.1.1. Range of a particle

In diffusion processes, in 3D, the mean squared distance of a particle to its original position $\boldsymbol{r}_0$ is given by $\langle(\boldsymbol{r} - \boldsymbol{r}_0)^2\rangle = 6Dt$. In 2D, $\langle(\boldsymbol{r} - \boldsymbol{r}_0)^2\rangle = 4Dt$. The mean squared distance for particles between plane membranes ($L = 10$) initially at the position $(x_0, y_0, z_0) = (5, 0, 0)$ were calculated at different time points. The results are shown in Fig. 4(d). At early times, the boundaries are too far to influence the motion of the particles, so they diffuse as if they were in a free 3D environment; therefore, $\langle(\boldsymbol{r} - \boldsymbol{r}_0)^2\rangle = 6Dt$. Eventually, the particles become uniformly distributed between the boundaries, and they diffuse in a 2D "plane" of thickness L; hence, $\langle(\boldsymbol{r} - \boldsymbol{r}_0)^2\rangle = 4Dt + L^2/12$. The term $L^2/12$ is added to take into account the uniform distribution of particles between the membranes. The transition between 3D and 2D diffusion is shown in Fig. 4(c) and (d). To illustrate the transition to 2D diffusion, the scales X and Y of Fig. 4(c) are the same. The transition is expected to occur when the particles reach the boundary, which is approximately when $Dt = L^2/24 \cong 4.17$.

5.2. Partially absorbing membrane at $x = 0$, reflecting membrane at $x = L$

The particles are initially located between a partially absorbing membrane with $k_1 = 1$ at $x = 0$ and a reflecting membrane ($k_2 = 0$) at $x = L = 10$.

In this case, the probability of binding is evaluated for each particle at each time step by using *Algorithm* 4. If a particle is free after a time step, its coordinate x is obtained by using *Algorithm* 3 and its coordinates y and z by generating Gaussian

[3] To simplify the discussion, dimensionless units are used.

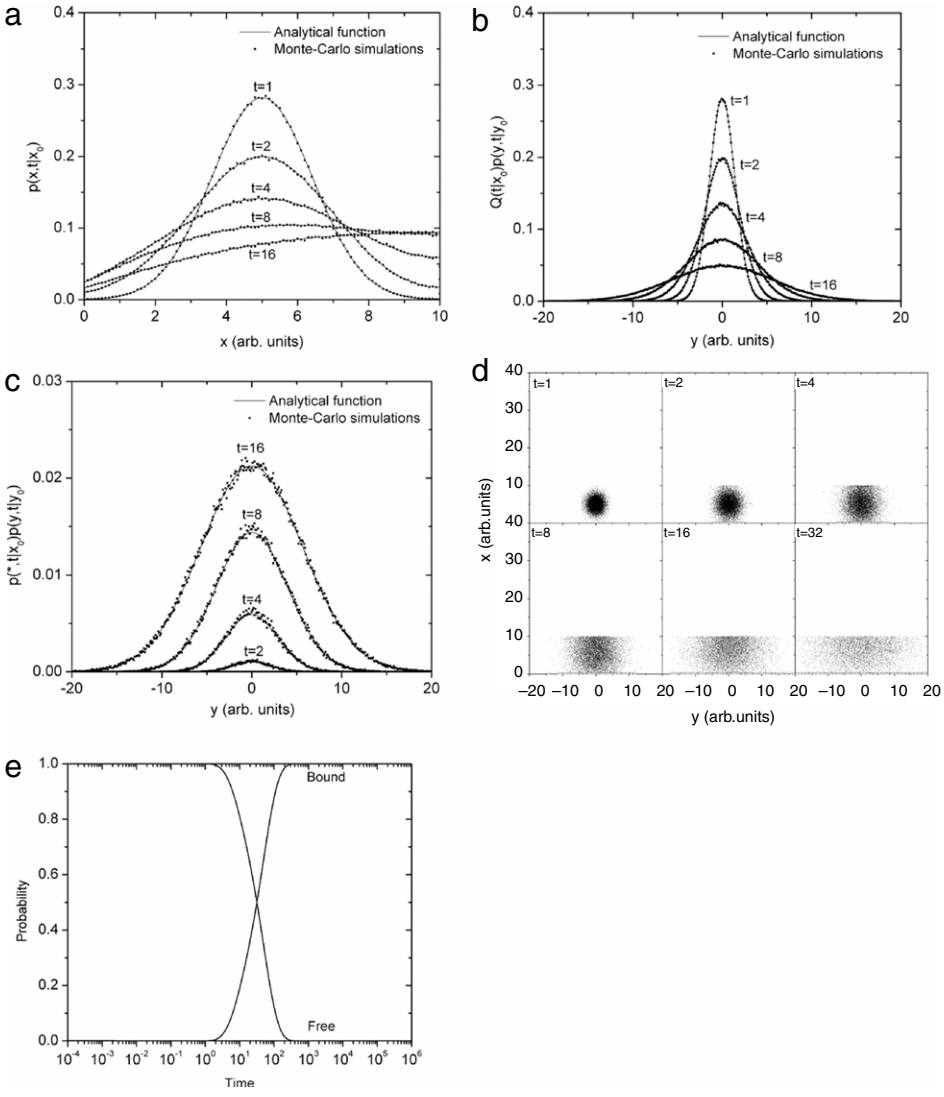

Fig. 5. Probability distributions $p_x(x, t \mid x_0)$ (panel a) and $Q(t \mid x_0)p_y(y, t \mid y_0)$ (panel b) for particles initially at $(x_0 = 5, y_0 = 0, z_0 = 0)$, diffusing freely between one partially absorbing membrane at $x = 0$ (with absorption rate constant $k_1 = 1$) and a reflecting membrane at $x = 10$, at $t = 1, 2, 4, 8$ and 16 units. Panel c: $p(*, t \mid x_0)p(y, t \mid y_0)$ for bound particles at $t = 2, 4, 8$ and 16 units. (−): Analytical predictions; (■): Monte Carlo simulations using 1,000,000 particles. Panel d: projection in the XY plane of the positions of particles (only 3000 are shown) used for the simulations depicted in panels a and b at $t = 1, 2, 4, 8, 16$ and 32 units. (·): free particles; (□) bound particles. Panel e: Survival and binding probabilities for the particles described in Fig. 5(a) and (b).

random numbers with variance $\sigma^2 = 2D\Delta t$ and mean $\mu = y_0$ and $\mu = z_0$. Otherwise, we consider the particle bounded.

In Fig. 5(d), the projection on the XY plane of the positions of particles initially at $(x_0, y_0, z_0) = (5, 0, 0)$, between the membranes at $x = 0$ and $x = L = 10$, is shown for $t = 1, 2, 4, 8, 16$ and 32 time units. At early times, the particles are not influenced by the membranes and their motion is similar to free diffusion in 3D. At $t = 4$, some particles interact with the membranes. Those close to the top are reflected, whereas those at the bottom may bind to the membrane. The coordinates of the particles are stored in histograms and normalized to the initial number of particles to yield the distributions of the coordinates in the directions X, Y and Z. The distributions in X and Y are shown in Fig. 5(a) and (b). To obtain the analytical distribution in one direction (such as X), we need to integrate $p(x, y, z, t \mid x_0, y_0, z_0)$ over Y and Z.[4] The integration of $p_y(y, t \mid y_0)$ and $p_z(z, t \mid z_0)$ over the domain is 1 for this system; therefore, the distribution of particles in X is $p_x(x, t \mid x_0)$. However, for the distribution in Y, the integration of the distribution over X yields the survival probability $Q(t \mid x_0)$, and the integration over Z is 1. Therefore, the distribution of coordinates of the particles in the direction Y is $Q(t \mid x_0)p_y(y, t \mid y_0)$. Similarly, the distribution in the direction Z (not shown) is $Q(t \mid x_0)p_z(z, t \mid z_0)$.

The probability that a particle at initial position (x_0, y_0, z_0) binds at $(x = 0, y, z)$ at time t is given by $p(*, y, z, t \mid x_0, y_0, z_0) = p(*, t \mid x_0)p_y(y, t \mid y_0)p_z(z, t \mid z_0)$. Once again an integration should be performed over the variable Z to get the distribution of bound particles in the direction Y. Therefore, the distribution of bound particles in the direction Y is $p(*, y, t \mid x_0, y_0) = p(*, t \mid x_0)p_y(y, t \mid y_0)$. Similarly, the distribution of bound particles in the direction Z (not shown) is $p(*, t \mid x_0)p_z(z, t \mid z_0)$. With time, all particles eventually bind to the absorbing membrane (Fig. 5(e)). As in Section 5.1, to further validate the sampling algorithm, a simulation was performed with membranes at $x = 0$ and $x = L = 100$, for particles at $(x_0 = 1, y_0 = 0, z_0 = 0)$, at $t = 1, 2, 4, 8$ and 16 units. In this case, $p_x(x, t \mid x_0)$ can be approximated by Eq. (7) of Ref. [17]. No significant difference was observed when the distributions of particles in X were compared to those predicted by this equation (results not shown).

[4] In that sense, there are the marginal distributions of $p(x, y, z, t \mid x_0, y_0, z_0)$.

Please cite this article in press as: I. Plante, et al., Calculations of distance distributions and probabilities of binding by ligands between parallel plane membranes comprising receptors, Computer Physics Communications (2013), http://dx.doi.org/10.1016/j.cpc.2013.09.011

Table 1
Simulation times of the algorithms for two reflecting membranes ($x_0 = 0.5$).

Parameters	*Algorithm* 1					*Algorithm* 2				
Dt	1	2	4	8	16	1	2	4	8	16
$L = 1$	30.1	–	–	–	–	22.3	13.5	9.36	6.80	5.04
$L = 5$	27.1	27.6	28.0	29.2	30.7	24.3	14.9	10.1	7.30	5.43
$L = 10$	27.2	27.4	28.1	27.9	28.9	28.7	17.3	11.9	8.13	5.90
$L = 20$	26.7	27.2	27.4	27.8	28.5	44.6	25.8	16.8	10.9	7.99
$L = 50$	24.5	24.7	27.5	27.5	28.3	130.0	71.0	40.1	23.2	14.6
$L = 100$	24.4	24.6	24.9	25.0	28.2	418.0	216.0	116.0	63.7	35.6

The gray shading indicates the fastest algorithm.

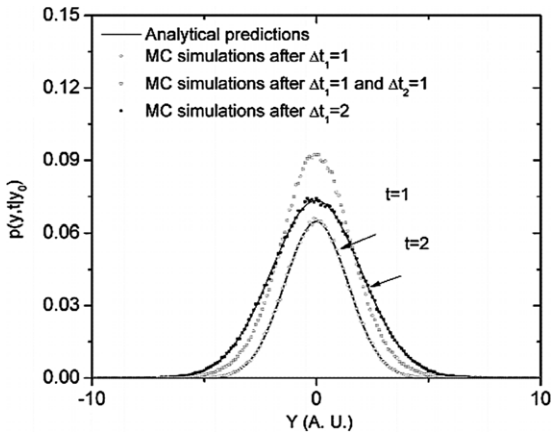

Fig. 6. Effect of the time steps on $Q(t \mid x_0)p_y(y, t \mid y_0)$ for bound particles. For this simulation, $k_1 = 1$, $x_0 = 1$ and $L = 5$. The simulation is attempted with two time steps ($\Delta t_1 = 1$ and $\Delta t_2 = 1$) and with one time step ($\Delta t_1 = 2$). The distribution obtained with two time steps is different (see text for details).

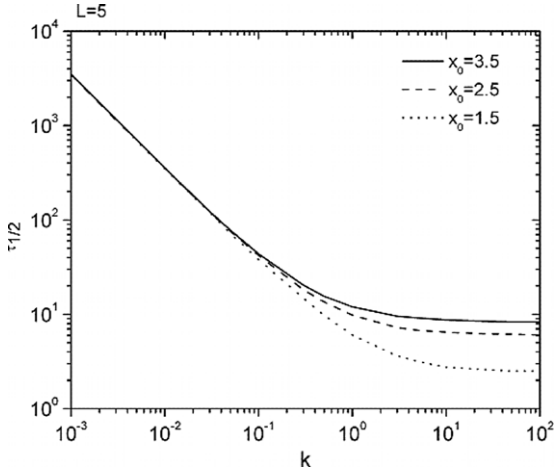

Fig. 7. Half life ($\tau_{1/2}$) of particles diffusing between the plane membranes $x = 0$ and $x = 5$, initially at $x_0 = 1.5$, 2.5 and 3.5 as a function of k_1.

5.2.1. Range of a particle

A goal of this calculation was to find how far particles located between two membranes will go, using the algorithms developed for this paper. This calculation assumes that the bound particles do not move.

However, as shown in Fig. 6, when this assumption is used for the calculation, the time discretization equations are not verified; therefore, the results are a function of the number of time steps used. The reason is that all particles diffuse in the directions Y and Z during the first time step (Δt_1). The simulation is over for the bound particles (they do not move anymore) and they are considered bound at $(0, Y, Z)$, Y and Z being the sampled values. Therefore, only the free particles are allowed to diffuse further during the second time step (Δt_2). If the simulation is done in one single time step ($\Delta t_1 + \Delta t_2$), the correct number of bound particles is found. However, the distribution of particles in the directions Y and Z are different, because no particles are bound initially and therefore all particles diffuse in the directions Y and Z during $\Delta t_1 + \Delta t_2$ in this case. To have the distribution of particles in the directions Y and Z obey the time discretization equations, the bound particles should be allowed to diffuse in the directions Y and Z with the diffusion coefficient used for free particles. However, in real cell cultures, it is unlikely that bound particles diffuse with the same diffusion coefficient in the directions Y and Z. This example illustrates the usefulness of the time discretization property in the description of the model system, which allows a systematic verification of the algorithms.

5.2.2. Lifetime of a particle

At last, the half life ($\tau_{1/2}$) of particles was calculated for particles diffusing between the membranes located at $x = 0$ and $x = 5$, for $x_0 = 1.5$, 2.5 and 3.5 and for k_1 varying from 10^{-3} to 10^2. The results are shown in Fig. 7. The half life is not dependent on the initial position of the particles for small values of k_1, because many particles are reflected by the reflecting and to some extent by the absorbing membrane. Therefore the particles have sufficient time to diffuse and reach nearly uniform distribution between the membranes before they bind. This is not true for larger values of k_1, because the probability of binding is so high that the particles will bind when they are near the boundary (instead of being reflected). Eventually, all the particles bind to the receptors in the system, regardless of the value of k_1.

5.3. Performance of the algorithms

We used the algorithms to simulate the trajectories of 1,000,000 particles on a computer with an Intel® Xeon® CPU E5-2640 @ 2.50 GHz. The simulation times for several values of Dt and L are given in Table 1.

Algorithm 1 was used only for $L^2 \geq (Dt) \ln 2$, whereas *Algorithm* 2 was used for all values of L and Dt. The fastest algorithm for a given combination of parameters is indicated by a grayed cell in the table. As discussed in Appendix B, the simulation times for *Algorithm* 1 are more or less constant, whereas those for *Algorithm* 2 increase with L^2/Dt. *Algorithm* 2 is faster than *Algorithm* 1 even for some cases where $L^2 \geq (Dt) \ln 2$.

In Table 2, the simulation times for the case of a partially absorbing membrane at $x = 0$, with association rate constant $k_1 = 1$ and reflecting membrane at $x = L$ are given. As in the previous case, 1,000,000 particle trajectories are simulated, using *Algorithms* 3 and 4.

The algorithms are very fast for small values of L and large values of Dt, because many particles bind to the absorbing boundary

Table 2
Simulation times of the algorithm for absorbing and reflecting membranes ($x_0 = 0.5$, $k_1 = 1$).

Parameters	*Algorithm* 3				
Dt	1	2	4	8	16
$L = 1$	9.30	7.21	5.27	3.57	3.18
$L = 5$	19.3	16.6	14.9	13.2	10.5
$L = 10$	29.5	25.1	22.2	18.9	16.8
$L = 20$	56.1	43.0	34.9	29.5	25.6
$L = 50$	222.0	124.0	80.3	58.8	47.3
$L = 100$	804.0	416	206.0	133.0	87.1

and, therefore, *Algorithm* 3 does not need to be used to sample the propagator. The calculation time also greatly increases with large values of L. In these cases, $p_x(x, t \mid x_0)$ takes a much simpler form (given by Eq. (7) of Ref. [17]), for which a faster sampling algorithm can be used.

6. Conclusion and perspectives

The Green's functions for particles located between parallel membranes are relevant to many fields in chemistry and biology. For example, in radiation chemistry, most existing simulation codes assume diffusion of particles in an infinite 3D medium [20,25,26]. However, it is certainly not the case in radiobiology, and it is important to simulate diffusion of particles in confined spaces for future biophysical models. Another example of this is the cell culture models [13–16]. The Green's functions are well known, but their evaluation and sampling are difficult because their analytical forms are complex. Despite these difficulties, exact algorithms were developed to sample these Green's functions and simulate the diffusion of a particle between membranes. It could be useful to use this approach in similar systems for which the analytical Green's functions are known [18], notably inside or outside a circular membrane representative of a cell and/or micro-tubules. This analytical method will be difficult to use in more complicated systems or geometries; eventually, most related problems will require numerical approaches. Nevertheless, the BD algorithms can be useful for several purposes, notably to benchmark future numerical calculations of the range and lifetime of a particle. We also remark that existing BD simulations use adaptive time-step algorithms [13,15]. This kind of algorithm may be difficult to use when a large number of particles are followed simultaneously. There are also some small discrepancies in the survival probability between previous BD simulations and analytical predictions [15].

An important application of the theory described in this paper is the study of the response of a group of cells to ionizing radiation, specifically the role of TGF-β. As ionizing radiation creates radical and molecular species ($^{\cdot}OH$, $H^{\cdot}$, H_2, H_2O_2, e^-_{aq}, ...) by the radiolysis of water in living matter [25], and as $^{\cdot}OH$ radicals liberate TGF-β molecules from their latent complex LTGF-β [10], this work should allow us to follow the evolution of TGF-β in cell culture or tissue models after irradiation. Indeed, activated TGF-β binds to cell receptors and initiates signal transduction by the activation of a cascade of downstream signaling events mediated by Smad proteins, which may result in several biological consequences [27]. In this perspective, the simulations described in this paper are another step in the implementation of a BD algorithm to explain the experimental results on the role of TGF-β in irradiated cell cultures or tissues.

In future work, radiation track structure models [28] in different geometries will be used to calculate the number of activated TGF-β in a cell culture and to include TFG-β signaling pathways in existing DNA repair models [29] and its role in controlling DNA damage responses [27]. Differences between high and low doses, and random interactions of X-rays or electrons versus the distinct track structures of high-energy ions will be investigated. Of importance in this model is the ability to simulate interactions at low doses where stochastic effects induced by a small number of molecules or interactions come into play. Eventually, these simulations will be used to calculate the range, lifetime and concentration of TGFβ following irradiation, as well as the number of cells affected by TGFβ and the positions where these molecules will bind to the cell surface receptors to initiate signal transduction. They are the cornerstone of a computational model that could allow a better understanding of cell communication in an irradiated system, and an approach to make predictions for conditions difficult to access by experiments, including the understanding of radiation effects at low doses of ionizing radiation. Another possible application of the algorithms is the simulation of signal transmission in a neuronal synapse. In this case, neurotransmitters are secreted by the presynaptic neuron and bind to the receptors located on the postsynaptic cell.

Acknowledgments

This work was supported by the NASA Space Radiation Risk Assessment Project, the DoE Low Dose Program (DE-AI02-09ER64843), and the University of Nevada, Las Vegas. We also thank the reviewers for their valuable comments.

Appendix A. Evaluation of integral

In this section, the integral

$$I = \int_0^L Z_n(x) Z_m(x) dx, \tag{A.1}$$

is evaluated for $Z_n(x)$ given by Eq. (15). The result is simply δ_{mn}. Expanding the integrand yields:

$$Z_n(x)Z_m(x) = \frac{\sqrt{2}\left[D\alpha_n \cos(\alpha_n x) + k_1 \sin(\alpha_n x)\right]}{\sqrt{\left(D^2\alpha_n^2 + k_1^2\right)L + Dk_1}} \times \frac{\sqrt{2}\left[D\alpha_m \cos(\alpha_m x) + k_1 \sin(\alpha_m x)\right]}{\sqrt{\left(D^2\alpha_m^2 + k_1^2\right)L + Dk_1}}. \tag{A.2}$$

This product gives four terms. To simplify expressions, we define the integrals I_1, I_2, I_3 and I_4 such that $I = I_1 + I_2 + I_3 + I_4$ and a common factor $C_{n,m}$:

$$C_{n,m} = \frac{2}{\sqrt{\left(D^2\alpha_n^2 + k_1^2\right)L + Dk_1}\sqrt{\left(D^2\alpha_m^2 + k_1^2\right)L + Dk_1}}, \tag{A.3}$$

$$I_1 = C_{n,m} D^2 \alpha_n \alpha_m \int_0^L \cos(\alpha_n x)\cos(\alpha_m x) dx, \tag{A.4a}$$

$$I_2 = C_{n,m} D \alpha_n k_1 \int_0^L \cos(\alpha_n x)\sin(\alpha_m x) dx, \tag{A.4b}$$

$$I_3 = C_{n,m} D \alpha_m k_1 \int_0^L \cos(\alpha_m x)\sin(\alpha_n x) dx, \tag{A.4c}$$

$$I_4 = C_{n,m} k_1^2 \int_0^L \sin(\alpha_n x)\sin(\alpha_m x) dx. \tag{A.4d}$$

These integrals yield different results, depending whether the values of α_n and α_m are equal or different. Therefore, the case $\alpha_n \neq \alpha_m$

is examined first:

$$I_1 = C_{n,m}D^2\alpha_n\alpha_m \times \left[\frac{\alpha_m\cos(\alpha_nL)\sin(\alpha_mL) - \alpha_n\cos(\alpha_mL)\sin(\alpha_nL)}{\alpha_m^2-\alpha_n^2}\right] \quad (A.5)$$

Using (17a) and (17b), this yields $I_1 = 0$.

$$I_2 = C_{n,m}D\alpha_nk_1 \times \left[\frac{\alpha_m - \alpha_m\cos(\alpha_mL)\cos(\alpha_nL) - \alpha_n\sin(\alpha_mL)\sin(\alpha_nL)}{\alpha_m^2-\alpha_n^2}\right], \quad (A.6)$$

$$I_3 = C_{n,m}D\alpha_mk_1 \times \left[\frac{-\alpha_n + \alpha_n\cos(\alpha_nL)\cos(\alpha_mL) + \alpha_m\sin(\alpha_mL)\sin(\alpha_nL)}{\alpha_m^2-\alpha_n^2}\right]. \quad (A.7)$$

Therefore

$$I_2 + I_3 = C_{n,m}Dk_1\sin(\alpha_mL)\sin(\alpha_nL) = C_{n,m}Dk_1 \times \left[\frac{k_1^2}{\sqrt{k_1^2+D^2\alpha_n^2}\sqrt{k_1^2+D^2\alpha_m^2}}\right]. \quad (A.8)$$

The last integral I_4 yields

$$I_4 = C_{n,m}k_1^2\left[\frac{\alpha_n\cos(\alpha_nL)\sin(\alpha_mL) - \alpha_m\cos(\alpha_mL)\sin(\alpha_nL)}{\alpha_m^2-\alpha_n^2}\right] = -C_{n,m}k_1^2\left[\frac{Dk_1}{\sqrt{k_1^2+D^2\alpha_n^2}\sqrt{k_1^2+D^2\alpha_m^2}}\right]. \quad (A.9)$$

From this, $I = I_1 + I_2 + I_3 + I_4 = 0$. If $\alpha_n = \alpha_m$, the integrals yield different results. We have:

$$I_1 = C_{n,n}D^2\alpha_n^2\left[\frac{\alpha_nL + \sin(\alpha_nL)\cos(\alpha_nL)}{2\alpha_n}\right], \quad (A.10)$$

$$I_2 = I_3 = C_{n,n}D\alpha_nk_1\left[\frac{\sin^2(\alpha_nL)}{2\alpha_n}\right], \quad (A.11)$$

$$I_4 = C_{n,n}k_1^2\left[\frac{\alpha_nL - \sin(\alpha_nL)\cos(\alpha_nL)}{2\alpha_n}\right]. \quad (A.12)$$

The sum of the terms is 1. Hence,

$$\int_0^L Z_n(x)Z_m(x)dx = \delta_{mn}. \quad (A.13)$$

Appendix B. Supplementary data

Supplementary material related to this article can be found online at http://dx.doi.org/10.1016/j.cpc.2013.09.011.

References

[1] M.H. Barcellos-Hoff, C. Park, E.G. Wright, Nat. Rev. Cancer 5 (2005) 867. http://dx.doi.org/10.1038/nrc1735.
[2] M.H. Barcellos-Hoff, Radiat. Res. Suppl. 150 (1998) S109. http://dx.doi.org/10.2307/3579813.
[3] C.B. Seymour, C. Mothersill, Nat. Rev. Cancer 4 (2004) 158. http://dx.doi.org/10.1038/nrc1277.
[4] K.M. Prise, M. Folkard, B.D. Michael, Radiat. Prot. Dosim. 104 (2003) 347. http://dx.doi.org/10.1093/oxfordjournals.rpd.a006198.
[5] D.I. Portess, G. Bauer, M.A. Hill, P. O'Neill, Cancer Res. 67 (2007) 1246. http://dx.doi.org/10.1158/0008-5472.CAN-06-2985.
[6] E.I. Azzam, S.M. De Toledo, D.R. Spitz, J.B. Little, Cancer Res. 62 (2002) 5436.
[7] H. Matsumoto, S. Hayashi, M. Hatashita, K. Ohnishi, H. Shioura, T. Ohtsubo, R. Kitai, T. Ohnishi, E. Kano, Radiat. Res. 155 (2001) 387. http://dx.doi.org/10.1667/0033-7587(2001)155[0387:IORBAN]2.0.CO;2.
[8] J.B. Little, E.I. Azzam, S.M. de Toledo, H. Nagasawa, Radiat. Prot. Dosim. 99 (2002) 159. http://dx.doi.org/10.1093/oxfordjournals.rpd.a006751.
[9] J.P. Annes, J.S. Munger, D.B. Rifkin, J. Cell Sci. 116 (2003) 217. http://dx.doi.org/10.1242/jcs.00229.
[10] M.F. Jobling, J.D. Mott, M.T. Finnegan, V. Jurukovski, et al., Radiat. Res. 166 (2006) 839. http://dx.doi.org/10.1667/RR0695.1.
[11] B. Schmierer, A.L. Tournier, P.A. Bates, C.S. Hill, Proc. Natl. Acad. Sci. 105 (2008) 6608. http://dx.doi.org/10.1073/pnas.0710134105.
[12] K.B. Ewan, R.L. Henshall-Powell, S.A. Ravani, M.J. Prarjes, C. Arteaga, R. Warters, R.J. Akhurst, M.H. Barcellos-Hoff, Cancer Res. 62 (2002) 5627.
[13] L. Batsilas, A.M. Berezhkovskii, S.Y. Shvartsman, Biophys. J. 85 (2003) 3659. http://dx.doi.org/10.1016/S0006-3495(03)74783-3.
[14] S.H. Wiley, S.Y. Shvartsman, D.A. Lauffenburger, Trends Cell Biol. 13 (2003) 43. http://dx.doi.org/10.1016/S0962-8924(02)00009-0.
[15] M.I. Monine, A.M. Berezhkovskii, E.J. Joslin, S.H. Wiley, D.A. Lauffenburger, S.Y. Shvartsman, Biophys. J. 88 (2005) 2384. http://dx.doi.org/10.1529/biophysj.104.051425.
[16] S.Y. Shvartsman, S.H. Wiley, W.H. Deen, D.A. Lauffenburger, Biophys. J. 81 (2001) 1854. http://dx.doi.org/10.1016/S0006-3495(01)75837-7.
[17] I. Plante, F.A. Cucinotta, Phys. Rev. E 84 (2011) 051920. http://dx.doi.org/10.1103/PhysRevE.84.051920.
[18] H.S. Carslaw, J.C. Jaeger, Conduction of Heat in Solids, Oxford University Press, Oxford, 1959.
[19] A.P.S. Selvadurai, Partial Differential Equations in Mechanics, Vol. 1, Springer-Verlag, New York, 2000.
[20] I. Plante, Radiat. Environ. Biophys. 50 (2011) 389. http://dx.doi.org/10.1007/s00411-011-0367-8.
[21] I. Plante, L. Devroye, F.A. Cucinotta, J. Comput. Phys. 242 (2013) 531. http://dx.doi.org/10.1016/j.jcp.2013.02.001.
[22] L. Devroye, Am. J. Math. Manage. Sci. 1 (1981) 359.
[23] L. Devroye, Non-Uniform Variate Generation, Springer-Verlag, New York, 1986. http://luc.devroye.org/rnbookindex.html.
[24] L. Devroye, Statist. Probab. Lett. 31 (1997) 2785.
[25] Y. Muroya, I. Plante, E.I. Azzam, J. Meesungnoen, Y. Katsumura, J.-P. Jay-Gerin, Radiat. Res. 165 (2006) 485. http://dx.doi.org/10.1667/RR3540.1.
[26] Y. Frongillo, T. Goulet, M.-J. Fraser, V. Cobut, J.P. Patau, J.-P. Jay-Gerin, Radiat. Phys. Chem. 51 (1998) 245. http://dx.doi.org/10.1016/S0969-806X(97)00097-2.
[27] M. Wang, J. Saha, M. Hada, J.A. Anderson, J.M. Pluth, P. O'Neill, F.A. Cucinotta, Nucleic Acids Res. 41 (2013) 933. http://dx.doi.org/10.1093/nar/gks1038.
[28] I. Plante, F.A. Cucinotta, in: C.J. Mode (Ed.), Applications of Monte Carlo Methods in Biology, Medicine and Other Fields of Sciences, Intech, Rijeka, Croatia, 2011, p. 315. http://dx.doi.org/10.5772/15674.
[29] F.A. Cucinotta, J.M. Pluth, J.A. Anderson, J.V. Harper, P. O'Neill, Radiat. Res. 169 (2008) 214. http://dx.doi.org/10.1667/RR1035.1.